Metal-coated concave cone in a fused-silica rod as a multi-function plasmonic element

Isabelle Verrier, Colette Veillas, Jean-Yves Michalon, Olivier Parriaux, Sebastian Henkel, Christian Schulze, Jens Bliedtner, Yves Jourlin

Optics Letters

Metal-coated concave cone in a fused-silica rod as a multi-function plasmonic element

Isabelle Verrier,[1,*] Colette Veillas,[1] Jean-Yves Michalon,[1] Olivier Parriaux,[1] Sebastian Henkel,[2] Christian Schulze,[2] Jens Bliedtner,[2] and Yves Jourlin[1]

[1]Université de Lyon, UJM Saint-Etienne, CNRS, Institut d'Optique Graduate School, Laboratoire Hubert Curien, UMR 5516, 18 rue du professeur Benoit Lauras, 42000 Saint-Etienne, France
[2]Ernst-Abbe-Hochschule Jena, University of Applied Sciences, Carl-Zeiss-Promenade 2, 07745 Jena, Germany
*Corresponding author: isabelle.verrier@univ-st-etienne.fr

Received 6 October 2022; revised 19 December 2022; accepted 22 December 2022; posted 22 December 2022; published 24 January 2023

A collimated light beam parallel to the axis of a fused-quartz cylinder impinging on a 90° apex angle concave cone cut in a quartz rod is transformed into a cylindrical wave by total internal reflection. A thin metal film at the quartz–air interface enables excitation of the plasmon mode at the air side that can polarize the cylindrical wave and/or has the potential to monitor physical, chemical, or biological quantities or events at the inner wall of the cone. The present Letter first analyzes the plasmon coupling mechanism and conditions. It then describes the diamond-grinding technique achieving a smooth cone wall and the finest possible tip. The experimental evidence of the polarization conversion is brought on a diamond-grinded section of fused-silica rod and gold coating of the concave wall.

https://doi.org/10.1364/OL.477486

Plasmonic sensors are currently widely used in the fields of physics, biology, and environment [1–3]. They have remarkable properties for non-contact measurements and can reach high sensitivities. The geometry of such sensors is diverse: cylindrical [4], spherical [5], or planar [6]. In the cylindrical case, optical fibers of few tens of micrometer diameter are often used to support the plasmon that can easily be excited by the guided wave [7]. In free space, in contrast, a cylinder with a diameter in the centimeter range is not well adapted as a substrate because of the difficulty of exciting a plasmon. To circumvent this difficulty, one solution consists in cutting a concave cone directly inside the cylinder and to metallize its surface. The advantage of such a passive optical element in the form of a concave cone lies in the possibility of transforming a circularly polarized collimated beam into a cylindrical wave of TE and/or TM polarization. The idea of a polarizing function is thus made possible by a simple metallic coating for the plasmon excitation that is identical to the "Kretschmann" configuration [8]. Furthermore, such geometry can be also useful for some applications where the sensor sensitivity must be enhanced by a larger interaction surface.

The objective of the present study is to show the feasibility of a simple plasmonic component with this particular geometry that, to our knowledge, was not considered in previous works. A conical element was used to generate a radially polarized cylindrical wave under the condition of Brewster reflection [9] as well as metallic reflection without plasmon excitation with an additional cylindrical polarizer [10]. The work presented here demonstrates that such function can simply be achieved by a monolithic element. Additionally, the component can be used as a sensor.

We first simulate surface plasmon resonance (SPR) in the metal-coated conical structure. Its fabrication is then described showing the difficulty of machining a concave cone in a silica cylinder (see Supplement 1). Next, the experimental characterization setup is described as well as the early experimental demonstration of plasmonic coupling and related polarization-selective absorption before concluding with some perspectives.

The fused silica cylinder is illuminated by a plane wave parallel to its axis (perpendicular to its input face), which is totally reflected by a concave cone of 90° apex angle by total internal reflection against air [Figs. 1(a) and 1(c)]. The system being of rotational symmetry around the cylinder axis, the equivalent model consists therefore in a locally plane surface illuminated by a plane wave under oblique incidence whose angle corresponds to that formed by the cylinder axis and the wall of the cone [i.e., 45°, Figs. 1(b) and 1(d)].

This is justified by the fact that the cylinder diameter is approximately a thousand times the wavelength and therefore the dimension of the cone is large enough to consider an incident plane wave at its surface. With a metal film at the air–silica interface, however, there are dissipation losses and, most importantly, the possibility of plasmon excitation.

To predict the behavior of the equivalent structure, the power of the electromagnetic field reflected by the plane surface under a given incident polarization was calculated numerically using the commercially available set of codes [11]. The maps of the intensities reflected by the concave cone diamond-cut in the silica cylinder and metallized with gold under TE and TM polarizations and 45° incidence are plotted in Fig. 2 versus the wavelength and metal thickness. The reflectivity under TE polarization (0.99) is almost constant in the wavelength range from 400 nm to 1 μm for gold thicknesses above 30 nm [Fig. 2(a)]. The minima of TM reflection (in blue) around the wavelength 600 nm

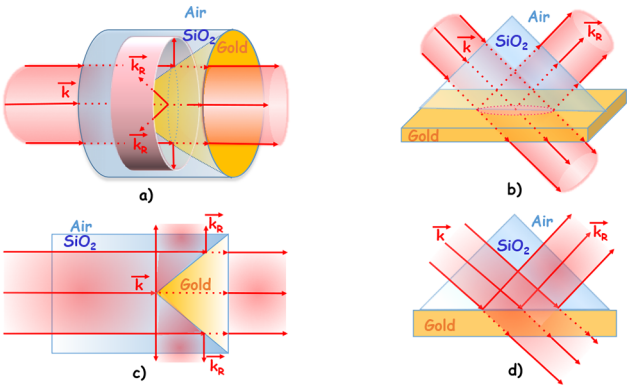

Fig. 1. Simulation model: (a) real structure; (b) planar equivalent; (c) and (d) cross sections of panels (a) and (b).

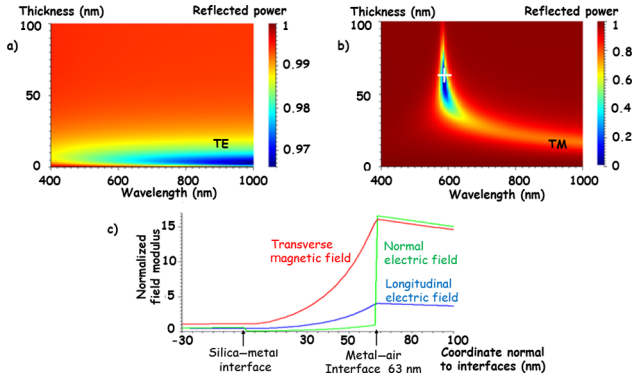

Fig. 2. Reflected power versus Au thickness and wavelength: (a) TE, see Data File 1 for underlying values; (b) TM polarizations, see Data File 2 for underlying values. (c) Field moduli at the silica–metal and metal–air interfaces, see Data File 3 for underlying values.

correspond to plasmon resonances, i.e., to the plasmon mode excitation at the metal–air interface [Fig. 2(b)]. This is proven by calculating the electromagnetic field under the condition of minimum reflection with a gold layer of 63 nm thickness normally to the interfaces at 586-nm wavelength as identified by the white cross in Fig. 2(b). The transverse magnetic field as well as the longitudinal electric field have their maximum at the metal–air interface as from there, all field components decrease slowly in the air medium with a field penetration depth $d = 258$ nm [Fig. 2(c)]. The plasmon propagation length $L = 9.2\,\mu m$, calculated using gold permittivity (Drude metal) and literature approximation [12], is large enough to reasonably consider sensor applications.

The plasmon resonance shifts toward smaller wavelengths when the gold thickness increases from 30 nm to 90 nm. Inside the blue zone of Fig. 2(b), the reflection minimum is obtained at the wavelength 586 nm for a thickness of 63 nm.

The structure fabrication consists of two steps: the machining of the cone and its metallization (Fig. 3).

The most difficult step is the machining of the 90° apex angle concave cone inside the fused silica cylinder of 9-mm diameter and 9.5-mm length (see Supplement 1). The result of the polished cone geometry can be seen in Figs. 4(a) and 4(b). It was possible to achieve the geometry requirements for the 90° apex angle. Three different gold thicknesses were deposited on three cones: 38 nm, 45 nm, and 63 nm [Fig. 4(c)].

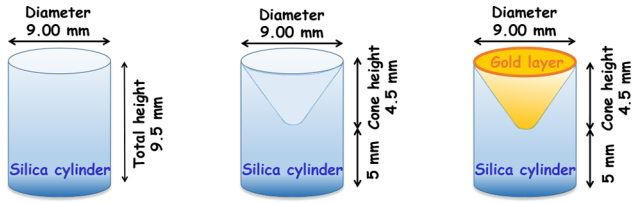

Fig. 3. Fabrication steps of the metallized concave cone structure.

The detection of the plasmon resonance effect on the cone reflection requires a specific measurement bench using a circularly polarized collimated excitation beam whose center coincides with the axis of the cylinder (Fig. 5). The incident light is a supercontinuum source whose spectral range is between 420 nm to 2.4 μm. The incident circularly polarized beam, obtained using a polarizer followed by a quarter-wave plate, excites simultaneously the TM and TE waves on the metallized cone with the same intensities. The cone reflects the collimated polychromatic incident beam, transforms it in a cylindrical wave, and enables the excitation of the plasmon resonance at its metal–air interface at a wavelength to be determined (Fig. 6). The analysis of the TE or TM polarized reflected wave was carried out using a linear polarizer set laterally to the cone. A collimator and an optical fiber connected to a miniature spectrometer then collect only a part of the cylindrical reflected beam under a small solid angle.

After a precise adjustment of the cylinder alignment, the resonance detection is carried out by the spectral analysis of a lateral portion of the reflected cylindrical wave (Fig. 7). The beam partially reflected by the beam splitter located between the quarter-wave plate and the cylinder was measured as the reference wave.

The normalized experimental spectra in reflection [Figs. 8(c) and 8(d)] are compared to those of the simulation for the TM and TE polarizations [Figs. 8(a) and 8(b)]. The shift between the measured resonance wavelengths λ_{Rexp} [Fig. 8(c)] and the simulated ones λ_{Rth} [Fig. 8(a)] could be explained by the theoretical permittivity values of gold taken from the software data library or by the inhomogeneous thickness deposited inside the cone whose wall is oriented at 45° from the evaporating source axis instead of 0° during fabrication. The full width at half maximum of each experimental resonance $\Delta\lambda_{1/2exp}$ seems larger than that calculated but these are preliminary results only showing the signature of the plasmon.

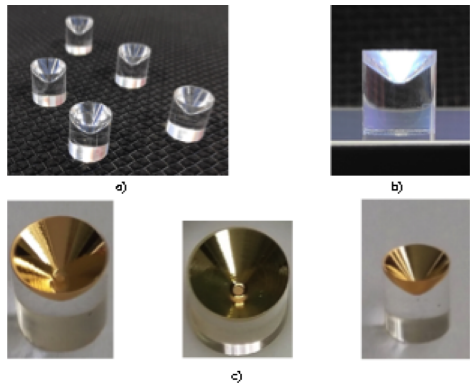

Fig. 4. Illustration of the concave cone structure: (a) polished component with high repeatability of the 90° angle; (b) polished component in sectional view; (c) metalized component.

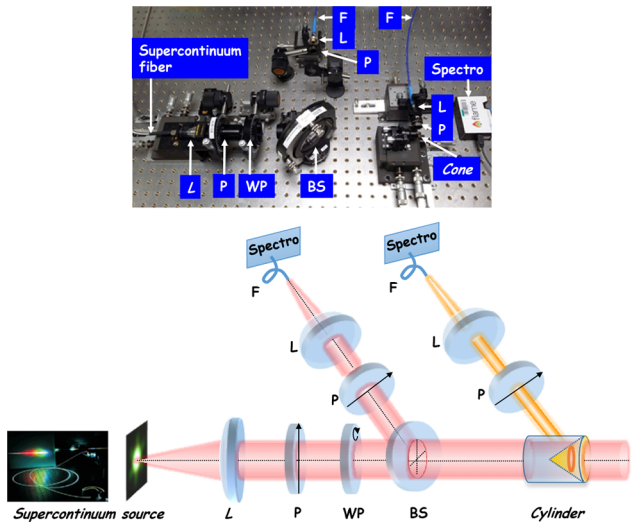

Fig. 5. Setup for plasmon resonance measurement. P, linear polarizer; WP, quarter-wave plate; L, lens; F, fiber.

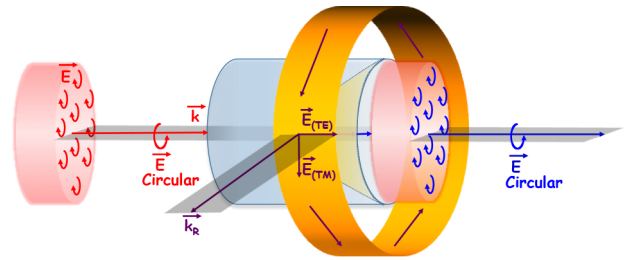

Fig. 6. Scheme of the polarization processing.

An enlarged view of the experimental resonance spectra of the TM polarization [Fig. 8(c)] is represented in Fig. 9 and permits to better appreciate the wavelength values, which are respectively measured at $\lambda_{Rexp} = 681$ nm, $\lambda_{Rexp} = 673$ nm, and $\lambda_{Rexp} = 656$ nm for gold thicknesses t = 38 nm, t = 45 nm, and t = 63 nm, respectively (instead of $\lambda_{Rth} = 616$ nm, $\lambda_{Rth} = 598$ nm, and $\lambda_{Rth} = 586$ nm in theory). The experimental full widths at half maximum of the resonances are as noted above somewhat larger than the theoretical ones: $\Delta\lambda_{1/2exp} = 50$ nm and $\Delta\lambda_{1/2exp} = 25$ nm instead of $\Delta\lambda_{1/2th} = 48$ nm and $\Delta\lambda_{1/2th} = 18$ nm for gold thicknesses of t = 45 nm and t = 63 nm. For a gold thickness t = 38 nm, the resonance width is difficult to evaluate because of the measurement accuracy.

Despite the resonance wavelength shift $\delta\lambda_R = \lambda_{Rexp} - \lambda_{Rth}$ between the measurements and the simulation, the TM reflectivity curves show the same trend: the plasmon resonance wavelength increases when the thickness decreases. Moreover, for each of the thicknesses (t = 38 nm, t = 45 nm, and t = 63 nm) $\delta\lambda_R$ remains identical ($\delta\lambda_R = 65$ nm, $\delta\lambda_R = 75$ nm,

Fig. 7. Alignment of the cone in front of the polarizer P and the fiber F.

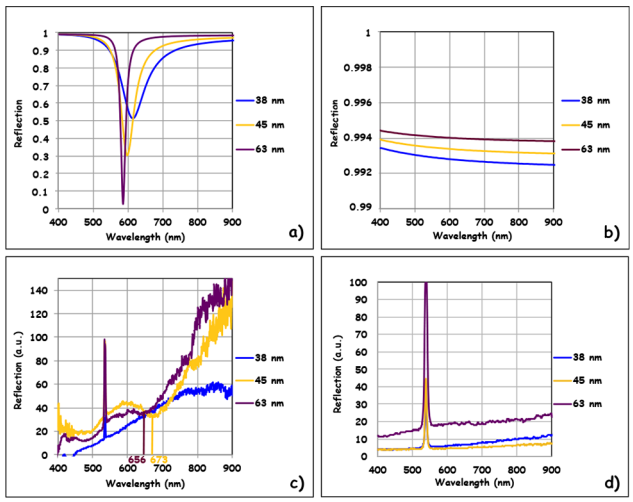

Fig. 8. Reflection spectra: (a) theoretical TM and (b) theoretical TE, see Data File 4 for underlying values; (c) measured TM and (d) measured TE, see Data File 5 for underlying values.

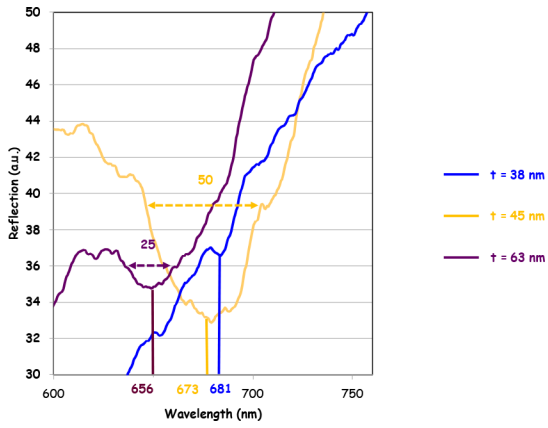

Fig. 9. Enlarged view of the measured TM reflection spectra [Fig. 8(c)].

and $\delta\lambda_R = 70$ nm) considering the measurement uncertainties and the modeling errors. The current optical resolution of the spectrometer is 1.5 nm. In addition, the error on the permittivity can lead to a very large systematic shift in resonance wavelength, which can go up to 100 nm according to the data table (Drude or Johnson–Christy) chosen from the software library as well as the error on the thicknesses that are probably not homogeneous and difficult to control. Thus, by considering all these errors or uncertainties, the plasmon excitation is effectively demonstrated experimentally by the minimal reflection observed on the TM polarization curves although the detector collects a very small part of the signal.

This article highlights the plasmon resonances effect at a metallized cone surface cut inside a silica cylinder of diameter approximately 1 centimeter. This monolithic element is simple and the main manufacturing difficulty is the machining of the concave cone inside the cylinder. An original measurement bench was designed to experimentally highlight the plasmon excitation along the cone surface at the metal–air interface and compare the results with the simulation. The question arises of the possibility of expanding the applicability of the analyzed

plasmon-coupling phenomenon to external media different from air, to water-based liquids in particular. This is possible indeed by changing the cylinder material whose refractive index, in the case of water, should be approximately 1.88. This suggests the use of high refractive index glasses or sulfur-containing polymers. Other materials for the cylinder, such as for example lanthanum glass, whose refractive index varies from 1.64 to 1.8, could be suitable with a different apex angle cone, thus widening the range of species detectable by the sensor and making it more versatile. Thereby, various uses can be envisaged for this passive component which authorizes the transformation of polarization and geometry of the beam or which is of interest for applications as an innovative plasmonic sensor due to its geometry.

Funding. Centre National de la Recherche Scientifique Renatech (Nano-SaintEtienne Platform); Région Auvergne Rhône Alpes France (PAR MICROSOLEN).

Acknowledgments. The authors thank Frédéric Arnould for the fabrication of the mechanical holders of the cone and polarizer.

Disclosures. The authors declare no conflicts of interest.

Data availability. Data underlying the results presented in this paper are available in Data File 1–Data File 5.

Supplemental document. See Supplement 1 for supporting content.

REFERENCES

1. S.A. Maier, *Plasmonics Fundamentals and Applications* (Springer, 2007).
2. J. Homola, Chem. Rev. **108**, 462 (2008).
3. B. Liedberg, C. Nylander, and I. Lunström, Sens. Actuators **4**, 299 (1983).
4. J. M. Nápoles-Duarte, M. A. Chavez-Rojo, M. E. Fuentes-Montero, L. M. Rodríguez-Valdez, R. García-Llamas, and J. A. Gaspar-Armenta, J. Opt. **17**, 065003 (2015).
5. A. G. M. da Silva, T. S. Rodrigues, J. Wang, L. K. Yamada, T. V. Alves, F. R. Ornellas, R. A. Ando, and P. H. C. Camargo, Langmuir **31**, 10272 (2015).
6. S. S. Hinman, K. S. McKeating, and Q. Cheng, Anal. Chem. **90**, 19 (2018).
7. W. Liu, Z. Liu, Y. Zhang, S. Li, Y. Zhang, and X. Yang, Opt. Laser Technol. **152**, 108167 (2022).
8. E. Kretschmann and H. Raether, Z. Naturforsch. **23**, 2135 (1968).
9. Y. Kozawa and S. Sato, Opt. Lett. **30**, 3063 (2005).
10. A. Shoham, R. Vander, and S. G. Lipson, Opt. Lett. **31**, 3405 (2006).
11. N. Lyndin and B. Usievich, *MC Grating Software* (2013).
12. W. L Barnes, J. Opt. A: Pure Appl. Opt. **8**, S87 (2006).